Research in Astron. Astrophys. **2010** Vol. **10** No. **10**, 1049–1060
http://www.raa-journal.org *http://www.iop.org/journals/raa*

Research in Astronomy and Astrophysics

Influence of coronal holes on CMEs in causing SEP events *

Cheng-Long Shen[1,2], Jia Yao[1], Yu-Ming Wang[1], Pin-Zhong Ye[1], Xue-Pu Zhao[3] and Shui Wang[1]

[1] CAS Key Laboratory of Basic Plasma Physics, School of Earth and Space Sciences, University of Science and Technology of China, Hefei 230026, China; *clshen@ustc.edu.cn; ymwang@ustc.edu.cn*
[2] State Key Laboratory of Space Weather, Chinese Academy of Science, Beijing 100080, China
[3] W. W. Hansen Experimental Physics Laboratory, Stanford University, Stanford, CA 94305, USA

Received 2010 March 5; accepted 2010 May 19

Abstract The issue of the influence of coronal holes (CHs) on coronal mass ejections (CMEs) in causing solar energetic particle (SEP) events is revisited. It is a continuation and extension of our previous work, in which no evident effects of CHs on CMEs in generating SEPs were found by statistically investigating 56 CME events. This result is consistent with the conclusion obtained by Kahler in 2004. We extrapolate the coronal magnetic field, define CHs as the regions consisting of only open magnetic field lines and perform a similar analysis on this issue for 76 events in total by extending the study interval to the end of 2008. Three key parameters, CH proximity, CH area and CH relative position, are involved in the analysis. The new result confirms the previous conclusion that CHs did not show any evident effect on CMEs in causing SEP events.

Key words: acceleration of particles — Sun: coronal mass ejections — Sun: coronal holes — Sun: particle emission

1 INTRODUCTION

Gradual solar energetic particle (SEP) events are thought to be a consequence of CME-driven shocks generating plenty of SEPs which would be observed near the Earth. In our previous work in 2006, we statistically studied the effect of coronal holes (CHs) on the CMEs in causing SEP events by investigating the location of the CME source and their relation with the CHs identified in EUV 284 Å (Shen et al. 2006, hereafter Paper I). It was implied that neither CH proximity nor CH relative location exhibits any evident effect on the intensities of SEP events. This result is consistent with the conclusion obtained by Kahler (2004), who comparatively studied the SEP events produced in the fast and slow solar wind streams and found no significant bias against SEP production in fast-wind regions which are believed to originate from CHs.

These findings do not seem to fit people's 'common sense' because CHs are believed to be regions with low-density and low temperature in the corona (e.g. Harvey & Recely 2002), from which the solar wind is fast and the magnetic field is open; therefore, apparently, three disadvantages

* Supported by the National Natural Science Foundation of China.

for a CME to produce SEP may exist when it is near a coronal hole region. These advantages are: (1) the background solar wind speed $V_{\rm sw}$ near CHs is larger than that in other regions; (2) the plasma density near CHs is much lower than that in other regions, so that the Alfvén speed $V_{\rm a}$ is larger (Shen et al. 2007; Gopalswamy et al. 2008); and (3) the magnetic field lines in CHs are open. The first two disadvantages suggest that a strong shock might hardly be produced near CHs. The third one implies that particles might be able to escape from the shock acceleration process earlier and easier. Thus, it can be expected that CHs would influence the CME in producing SEP events. The work by Kunches & Zwickl (1999) was consistent with the picture depicted above. In their paper, they found that the CH may delay the onset times of SEPs when a CH is present between the Sun-observer line and the solar source of the SEP event. They also speculate that the peak intensity could be influenced by the CH. However, they did not statistically study such an influence. It is hard to say if their conclusion is statistically significant.

In principle, CHs are open field regions, though they were first identified in observations (e.g. Zirker 1977). Kunches & Zwickl (1999) identified CHs based on He 10830 Å. In our 2006 work (Paper I), CHs were auto-determined based on EUV 284 Å images taken by SOHO/EIT. Thus, it is doubtful whether or not the CHs identified in EUV wavelengths really represent open field regions. Another doubt in our 2006 work is that only frontside CHs are taken into account. In order to remove the doubt and get a more reliable result, we look into this topic again by extrapolating the coronal magnetic field instead of analyzing EUV images. The term 'CHs' in this paper therefore actually refers to open field regions. The magnetic field extrapolation and determination of CHs are introduced in Section 2. Section 3 presents the statistical analysis. A brief summary and conclusions are given in Section 4.

2 DETERMINATION OF CORONAL HOLES

So far, there are no observations of the coronal magnetic field. Most information of the coronal magnetic field comes from various extrapolation techniques (e.g. Schatten et al. 1969; Altschuler & Newkirk 1969; Schatten 1971; Zhao & Hoeksema 1992, 1994, 1995; Zhao et al. 2002). In this paper, the current sheet-surface source (CSSS) model developed by Zhao and his colleagues (Zhao & Hoeksema 1995; Zhao et al. 2002) will be used to extrapolate the coronal magnetic field and identify the coronal hole regions. In our calculation, the daily-updated synoptic charts of the photospheric magnetic field from the Michelson Doppler Imager (MDI (Scherrer et al. 1995)) onboard the SOHO spacecraft is adopted as the bottom boundary condition; the extrapolated global magnetic field is a kind of average over the carrington rotation, and may not exactly reflect the state at the time of interest. However, because CHs are long-lived structures in the solar atmosphere, we think that such an approximation of the global field would not significantly distort our results. To determine where the open field regions are, we design a 180-by-90 grid of points (with a point every 2 degrees in longitude and 1/45 in sine latitude) over the photosphere as the roots of magnetic field lines. In other words, a total of 16200 field lines will be traced to check if they are open or closed.

By using this method, CHs are defined as the regions consisting of open magnetic field lines on the photosphere. Neighboring regions with a spherical separation distance $\leq 7.5^\circ$ are grouped into one region. Those small regions with an area less than $0.0024\,A_{\rm s}$ were discarded to raise the credibility of the determined CHs. Here $A_{\rm s}$ is the total area of the solar surface. The size of $0.0024\,A_{\rm s}$ is about a $10^\circ \times 10^\circ$ grid at the center of the solar disk (the projection of the Sun on the plane of sky). The projection effect has been corrected in the calculation of the area of open magnetic field regions. Compared with the previous approach developed by Shen et al. (2006), this method can not only obtain all CHs over the full solar surface (not just those on the front-side solar disk), but also extract the CHs covered by some bright structures (e.g., active regions) in EIT 284 Å images.

Figure 1 shows an example on 2000 September 16 which was also presented in Paper I. The asterisks in Figure 1(a) denote the open field regions inferred by the method (the Carrington map

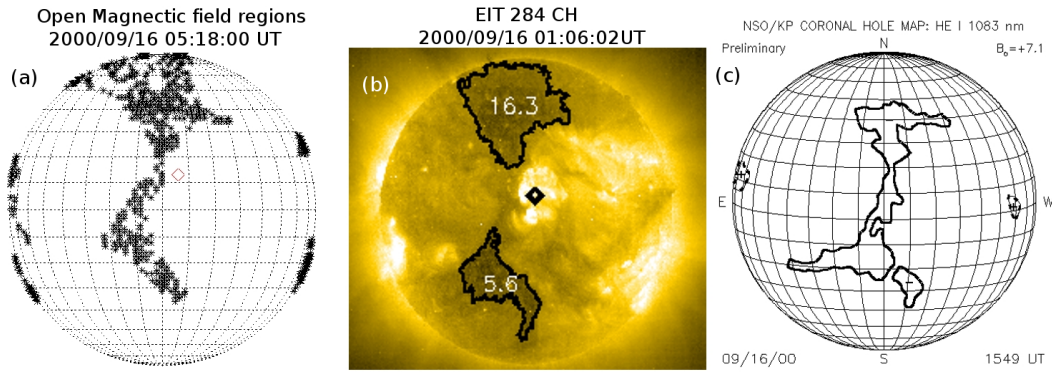

Fig. 1 (a) An example from 2000 September 16 showing CH determination by our method; the regions marked by crosses are the determined CHs, and the diamond indicates the CME location. (b) The corresponding EIT 284 Å image superimposed with CH boundaries obtained by the method in Paper I, (c) Kitt Peak CH map.

has been re-mapped onto the solar sphere). Figure 1(b) and (c) show the corresponding EIT 284 Å image over-plotted with the CH boundaries determined in Paper I and the Kitt Peak CH map for comparison.

It is obvious that CHs obtained here are similar to, but not the same as, those in the other two studies. The CHs presented in the EIT 284 Å are in the high corona and the Kitt Peak CHs are in the lower corona (Harvey & Recely 2002), whereas our extrapolated CHs are on the photosphere. Since CHs may expand rapidly and superradially with increasing height (Munro & Jackson 1977; Fisher & Guhathakurta 1995; DeForest et al. 2001), the difference in altitude between them is probably one of the major causes of the apparent difference in the CH shape. The regions determined here could be treated as the roots of the CHs. Moreover, the CHs at the east and west limbs in Figure 1(a) and (c) cannot be recognized in Figure 1(b). This is because of the shielding of the brightness of the nearby active region. In addition, the same CH also exhibits different shapes and properties in different panels. The big CH extending from north to south in the central longitude region shown in Figure 1(a) and (c) has been divided into two separated CHs in Figure 1(b). This may also be because the brightness of the active region shields the dark region located at the solar center, which makes this big CH resemble two isolated dark regions.

3 STATISTICAL RESULTS

In this paper, the time period of 1997–2003 we used in paper I is extended to the end of 2008. All fast halo CME events originating from the west hemisphere during this period are studied. Like we did in Paper I, the 'fast' and 'halo' mean that the CME projected speed measured in SOHO/LASCO is larger than 1000 km s^{-1} and the span angle is larger than 130°. Since the daily-updated magnetic field synoptic chart on 1998 November 5 is not available for use, the event that occurred on that day is excluded. Thus, a total of 76 events will be analyzed. Table 1 lists the events including the parameters of CMEs, CHs and SEPs. The key parameters we used to analyze the effect of CHs on CMEs in producing SEPs are the CH proximity (Col. (7)), the area of the CH nearest to the CME (Col. (8)) and the relative position of the CH (Col. (9)). All parameters have the same meaning as those in Paper I.

Table 1 Frontside Fast Halo CMEs Originating from the West Hemisphere during 1997–2008

No.	CME[a]					CH		SEP		
	Date	Time	Width ($^\circ$)	Speed (km s^{-1})	Location[b]	Proximity[c] (R_s)	Area[d] (A_s)	P[e]	$\geq$10MeV[f] (pfu)	$\geq$50MeV[g] (pfu)
(1)	(2)	(3)	(4)	(5)	(6)	(7)	(8)	(9)	(10)	(11)
1	1997–11–06	12:10:41	360	1556	S18, W62	0.60(D)	0.0049(a)	N	490.0	116.0
2	1998–04–20	10:07:11	165	1863	S47, W70	0.28(d)	0.0041(a)	Y	1610.0	103.0
3	1998–05–06	08:29:13	190	1099	S15, W68	0.54(D)	0.0066(A)	Y	239.0	19.3
4	1999–06–04	07:26:54	150	2230	N19, W85	0.86(D)	0.0053(a)	Y	64.0	0.9
5	1999–06–28	21:30:00	360	1083	N23, W42	0.51(D)	0.0070(A)	Y	–1.0	–1.0
6	1999–09–16	16:54:00	147	1021	N42, W30	0.31(d)	0.0045(a)	Y	–1.0	–1.0
7	2000–02–12	04:31:00	360	1107	N13, W28	0.51(D)	0.0116(A)	Y	2.7	–1.0
8	2000–04–04	16:32:00	360	1188	N16, W60	0.07(d)	0.0034(a)	N	55.8	0.3
9	2000–05–15	16:26:00	>165	1212	S23, W68	0.87(D)	0.0028(a)	Y	1.0	–1.0
10	2000–06–10	17:08:00	360	1108	N22, W40	0.25(d)	0.0059(a)	Y	46.0	6.5
11	2000–06–25	07:54:00	165	1617	N10, W60	0.31(d)	0.0066(A)	N	4.6	–1.0
12	2000–06–28	19:31:00	>134	1198	N24, W85	0.05(d)	0.0119(A)	Y	–1.0	–1.0
13	2000–07–14	10:54:00	360	1674	N17, W 2	0.97(D)	0.0101(A)	Y	24000.0	1670.0
14	2000–09–12	11:54:00	360	1550	S14, W 6	0.69(D)	0.0037(a)	Y	321.0	2.0
15	2000–09–16	05:18:00	360	1215	N13, W 6	0.11(d)	0.0296(A)	Y	7.1	–1.0
16	2000–11–08	23:06:00	>170	1738	N14, W64	0.88(D)	0.0045(a)	N	14800.0	1880.0
17	2000–11–24	15:30:00	360	1245	N21, W12	0.30(d)	0.0025(a)	Y	94.0	5.0
18	2001–02–11	01:31:00	360	1183	N21, W60	0.19(d)	0.0056(a)	N	–1.0	–1.0
19	2001–04–02	22:06:00	244	2505	N16, W65	0.54(D)	0.0103(A)	Y	1110.0	53.5
20	2001–04–09	15:54:00	360	1192	S20, W 4	1.06(D)	0.0081(A)	Y	5.9	1.2
21	2001–04–10	05:30:00	360	2411	S20, W10	1.07(D)	0.0065(A)	Y	355.0	3.7
22	2001–04–12	10:31:00	360	1184	S20, W43	1.00(D)	0.0102(A)	Y	50.5	5.8
23	2001–04–15	14:06:00	167	1199	S20, W85	1.03(D)	0.0111(A)	N	951.0	275.0
24	2001–04–26	12:30:00	360	1006	N23, W 2	0.83(D)	0.0128(A)	Y	57.5	–1.0
25	2001–07–19	10:30:00	166	1668	S 9, W61	0.36(D)	0.0033(a)	Y	–1.0	–1.0
26	2001–10–01	05:30:00	360	1405	S20, W89	0.25(d)	0.0054(a)	Y	2360.0	24.5
27	2001–10–22	15:06:00	360	1336	S18, W20	1.02(D)	0.0081(A)	N	24.2	2.5
28	2001–10–25	15:26:00	360	1092	S18, W20	0.32(D)	0.0049(a)	Y	–1.0	–1.0
29	2001–11–04	16:20:00	360	1274	N 6, W18	0.58(D)	0.0036(a)	Y	31700.0	2120.0
30	2001–11–22	23:30:00	360	1437	S17, W35	0.14(d)	0.0046(a)	N	18900.0	162.0
31	2001–12–26	05:30:00	>212	1446	N 9, W61	0.27(d)	0.0047(a)	N	780.0	180.0
32	2002–04–17	08:26:00	360	1218	N13, W12	0.22(d)	0.0068(A)	Y	24.1	0.4
33	2002–04–21	01:27:00	241	2409	S18, W79	0.06(d)	0.0081(A)	Y	2520.0	208.0
34	2002–05–22	03:50:00	360	1494	S15, W70	0.73(D)	0.0065(A)	Y	820.0	1.1
35	2002–07–15	20:30:00	360	1132	N20, W 2	0.08(d)	0.0164(A)	Y	234.0	0.9
36	2002–07–18	08:06:00	360	1099	N20, W33	0.05(d)	0.0098(A)	Y	14.2	0.6
37	2002–08–06	18:25:00	134	1098	S38, W18	0.31(d)	0.0040(a)	Y	–1.0	–1.0
38	2002–08–14	02:30:00	133	1309	N10, W60	0.04(d)	0.0083(A)	N	26.4	–1.0
39	2002–08–22	02:06:00	360	1005	S14, W60	0.46(D)	0.0035(a)	N	36.4	6.0
40	2002–08–24	01:27:00	360	1878	S 5, W89	0.28(d)	0.0041(a)	Y	317.0	76.2
41	2002–11–09	13:31:00	360	1838	S 9, W30	0.42(D)	0.0105(A)	Y	404.0	1.5
42	2002–12–19	22:06:00	360	1092	N16, W10	0.58(D)	0.0170(A)	Y	4.2	–1.0
43	2002–12–21	02:30:00	225	1072	N30, W 0	0.75(D)	0.0190(A)	Y	–1.0	–1.0
44	2002–12–22	03:30:00	272	1071	N24, W43	0.69(D)	0.0224(A)	Y	–1.0	–1.0
45	2003–03–18	12:30:00	209	1601	S13, W48	0.14(d)	0.0199(A)	Y	0.8	–1.0
46	2003–03–19	02:30:00	360	1342	S13, W56	0.17(d)	0.0212(A)	N	–1.0	–1.0
47	2003–05–28	00:50:00	360	1366	S 5, W25	0.12(d)	0.0044(a)	Y	121.0	0.3
48	2003–05–31	02:30:00	360	1835	S 5, W65	0.18(d)	0.0034(a)	Y	27.0	2.3
49	2003–10–26	17:54:00	>171	1537	N 3, W43	0.15(d)	0.0032(a)	Y	466.0	10.4
50	2003–10–27	08:30:00	>215	1380	N 3, W48	0.08(d)	0.0028(a)	Y	52.0	9.6
51	2003–10–29	20:54:00	360	2029	S16, W 5	0.72(D)	0.0027(a)	Y	2470.0	389.0
52	2003–11–02	09:30:00	360	2036	S16, W51	0.07(d)	0.0035(a)	N	30.0	0.8
53	2003–11–02	17:30:00	360	2598	S16, W56	0.08(d)	0.0035(a)	N	1570.0	155.0
54	2003–11–04	19:54:00	360	2657	S16, W83	0.07(d)	0.0037(a)	Y	353.0	15.3
55	2003–11–11	13:54:00	360	1315	S 3, W63	0.24(d)	0.0049(a)	Y	–1.0	–1.0

Table 1 – *Continued.*

No.	CME[a]					CH			SEP	
	Date	Time	Width	Speed	Location[b]	Proximity[c]	Area[d]	P[e]	≥10MeV[f]	≥50MeV[g]
			(°)	(km s^{-1})		(R_s)	(A_s)		(pfu)	(pfu)
(1)	(2)	(3)	(4)	(5)	(6)	(7)	(8)	(9)	(10)	(11)
56	2004–04–08	10:30:19	360	1068	S16, W 6	0.02(d)	0.0033(a)	Y	–1.0	–1.0
57	2004–07–25	14:54:05	360	1333	N 3, W33	0.72(D)	0.0028(a)	Y	54.6	0.8
58	2004–07–29	12:06:05	360	1180	N 0, W89	0.32(D)	0.0060(a)	Y	–1.0	–1.0
59	2004–07–31	05:54:05	197	1192	N 9, W89	0.37(D)	0.0059(a)	Y	–1.0	–1.0
60	2004–11–07	16:54:05	360	1759	N 9, W16	0.38(D)	0.0220(A)	Y	495.0	4.7
61	2004–11–09	17:26:06	360	2000	N 8, W48	0.31(d)	0.0270(A)	Y	82.4	0.9
62	2004–11–10	02:26:05	360	3387	N 7, W53	0.12(d)	0.0259(A)	Y	424.0	13.5
63	2004–12–03	00:26:05	360	1216	N 9, W 1	0.35(D)	0.0028(a)	Y	3.2	–1.0
64	2005–01–15	23:06:50	360	2861	N13, W 3	0.76(D)	0.0112(A)	Y	365.0	12.8
65	2005–01–17	09:30:05	360	2094	N13, W20	0.46(D)	0.0245(A)	Y	269.0	4.0
66	2005–01–17	09:54:05	360	2547	N13, W20	0.46(D)	0.0245(A)	Y	5040.0	387.0
67	2005–01–19	08:29:39	360	2020	N13, W45	0.51(D)	0.0246(A)	Y	–1.0	–1.0
68	2005–02–17	00:06:05	360	1135	S 1, W19	0.02(d)	0.0059(a)	Y	–1.0	–1.0
69	2005–07–09	22:30:05	360	1540	N 9, W29	0.31(d)	0.0313(A)	Y	3.0	–1.0
70	2005–07–13	14:30:05	360	1423	N 9, W76	0.33(D)	0.0382(A)	Y	12.5	0.3
71	2005–07–14	10:54:05	360	2115	N 9, W87	0.39(D)	0.0395(A)	Y	134.0	2.6
72	2005–08–22	01:31:48	360	1194	S12, W51	0.18(d)	0.0027(a)	Y	7.3	–1.0
73	2005–08–22	17:30:05	360	2378	S12, W60	0.18(d)	0.0027(a)	N	337.0	4.8
74	2005–08–23	14:54:05	360	1929	S13, W75	0.24(d)	0.0035(a)	Y	–1.0	–1.0
75	2006–12–13	02:54:04	360	1774	S 8, W19	0.14(d)	0.0027(a)	Y	698.0	239.0
76	2006–12–14	22:30:04	360	1042	S10, W42	0.19(d)	0.0032(a)	Y	215.0	13.5

[a] Obtained from CME CATALOG (*http://cdaw.gsfc.nasa.gov/CME_list/*).
[b] CME locations determined by the EIT movie.
[c] Shortest surface distance between a CME and a CH (from the CME site to the CH boundary) in units of $R_\odot$, called CH-proximity. 'D' means CH proximity is larger than 0.3 R_s while 'd' means it has other values.
[d] Area of the closest CH in units of A_s, the area of the solar surface. 'A' means the CH area larger is than 0.0061 A_s while 'a' means it is smaller than 0.0061 A_s.
[e] Relative location of a CH to the corresponding CME. 'Y' means the CH extends into the longitudes between the CME and the field lines connecting Earth to the Sun at about $W60°$, and 'N' indicates the CH is outside the two longitudes.
[f] Peak fluxes of $\geq$ 10 MeV-protons in units of pfu.
[g] Peak fluxes of $\geq$ 50 MeV-protons in units of pfu.

It should be noted that the parameters of CHs we obtained in this paper were different from Paper I, which may be caused by the following reasons:

1. The nearest CHs for a large number of events were changed:
   (a) As shown in Figure 1, the dark regions of CHs shielded by the brightness of an active region in EIT 284 Å images can be obtained in this paper. This makes the nearest CHs change in 26 events.
   (b) CHs located in the solar limb and backside have also been taken into account in this paper as we discussed in Section 2. In this paper, the nearest CHs changed to the limb or backside CHs in a total of 14 events.
2. For the other 15 events, the same CHs as those in this paper and paper I were used. It is found that the areas of these 15 CHs were smaller than what we obtained in paper I. In this paper, the CH we obtained can be treated as the roots of the CHs. Since CHs may expand rapidly and superradially with increasing height (Munro & Jackson 1977; Fisher & Guhathakurta 1995; DeForest et al. 2001), such a result could be expected.

Such variations make the properties of the nearest CHs show large changes. As we discussed before, the nearest CHs showed changes in a total of 40 events. Even for the same CH, the difference in the CH shape and different CH heights also make the properties of the nearby CHs change. In this paper, the relative positions of 26 events changed, and 20 events were changed from 'N' to 'Y.' Because of variation in the nearest CHs and the height and shape of some CHs, the group of CH areas and their proximities would be hard to compare.

For simplicity and reliability, we binarize the key parameters before further analysis. The events with a CH proximity larger than 0.31 $R_{\rm s}$ are marked as 'D' and the others are marked as 'd.' The events with the CH area larger/smaller than 0.0061 $A_{\rm s}$ are marked as 'A'/'a'. The parameter of the CH relative position is already bi-valued. The separation values 0.31 $R_{\rm s}$ and 0.0061 $A_{\rm s}$ are chosen to make the events nearly equally divided into two groups for the CH proximity and area, respectively. In the following subsections, we will present the analysis of these difference parameters.

3.1 Dependence of CH Proximity

Figure 2 shows the occurrence probabilities, P, of SEP events in terms of the CH proximity for proton energies $\geq$10 MeV (Panel a) and $\geq$50 MeV (Panel b). The SEP events at difference flux levels are presented by difference bins. For the SEP event with proton energy $\geq$ 10 MeV, the three levels are all SEP events, SEP events with proton flux $\geq$10 pfu and $\geq$100 pfu, in which 1 pfu = 1

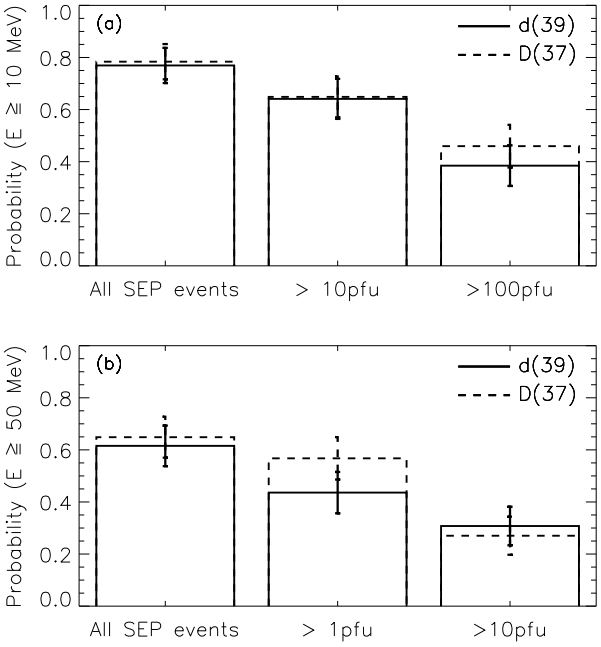

Fig. 2 Occurrence probabilities, P, of SEP events in terms of the CH proximity for proton energies $\geq$10 MeV (a) and $\geq$50 MeV (b). The probabilities of different groups are indicated by solid and dashed lines with error bars, respectively. Difference bins show the probabilities of different flux levels. For the SEP at energies $\geq$10 MeV, three levels are all SEP events, $\geq$10 and $\geq$100 pfu events, in which 1 pfu = 1 particle cm^{-2} s^{-1} sr^{-1}. For the SEP at energies $\geq$50 MeV, they are all SEP events, $\geq$1 and $\geq$10 pfu events.

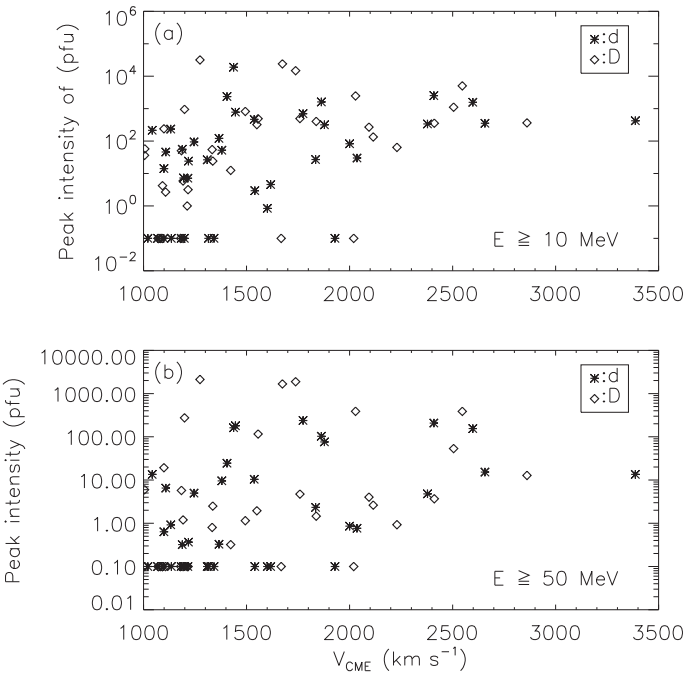

Fig. 3 Peak intensity of protons with energy $\geq$ 10 MeV vs. associated CME speed for proton energy $\geq$10 MeV (a) and $\geq$50 MeV (b). The asterisks show the CME events in group 'd' while diamonds show the CME events in group 'D'. Points at the peak intensity of 0.01 means no SEP is associated.

particle cm^{-2} s^{-1} sr^{-1}. For the SEP event with proton energy $\geq$ 50 MeV, they are all SEP events with proton flux $\geq$ 1 pfu and $\geq$ 10 pfu. Different lines show the probabilities in different groups. The probabilities at group 'd' and 'D' are indicated by solid and dashed lines with error bars, respectively. The CME number in each group is marked in the bracket at the top right of the figure. The error bars indicate the one standard deviation (σ) level, which is given by $\sigma = \sqrt{P(1-P)/N}$, where N is the total number of CME events for the corresponding bin.

It is found that the differences of occurrence probabilities of SEP events between these two groups are small for all flux and energy levels. All differences between these two groups are less than the value of the standard deviation (1σ). Such analysis confirms the result we obtained in paper I that CH proximity has no evident effect on CMEs in producing SEP events.

Furthermore, the correlation between the peak intensities of SEP events and the speed of associated CMEs is studied (shown in Fig. 3). Asterisks in Figure 3 show the events in group 'd' and diamonds show the events in group 'D.' Points at peak intensity of 0.01 mean no SEP event is associated (called SEPNCMEs for short). Panels (a) and (b) in this figure show the events with proton energy $\geq$10 MeV and $\geq$50 MeV, respectively. From this figure, it is found that the SEP associated CMEs (called SEPYCMEs in short) were faster than SEPNCMEs. Almost all (15/16) extremely fast CMEs with speed $\geq$2000 km s^{-1} were associated with SEP events.

Table 2 gives the comparison of the speed of CMEs in different groups. Different columns show the mean value of the CME speed of different groups binarized by CH proximity, CH area and relative position respectively. The first and second rows show the value of SEPYCMEs and SEPNCMEs for the SEP event with proton energy $\geq$10 MeV , while the third and fourth rows show them for proton energy $\geq$ 50 MeV respectively.

Table 2 Mean Value of CME Speed for Different Groups (in units of km s^{-1})

Energy	SEP	CH Proximity		CH area		Relative Position	
		d	D	a	A	Y	N
≥10 MeV	Y	1663±560[a]	1623±524	1604±454	1682±614	1655±559	1603±474
	N	1254±274	1297±353	1262±282	1298±369	1276±324	1263±112
≥50 MeV	Y	1726±605	1727±518	1650±459	1817±655	1755±574	1629±511
	N	1318±251	1232±288	1250±249	1305±292	1264±280	1363±183

[a] The number after ± shows the standard variation.

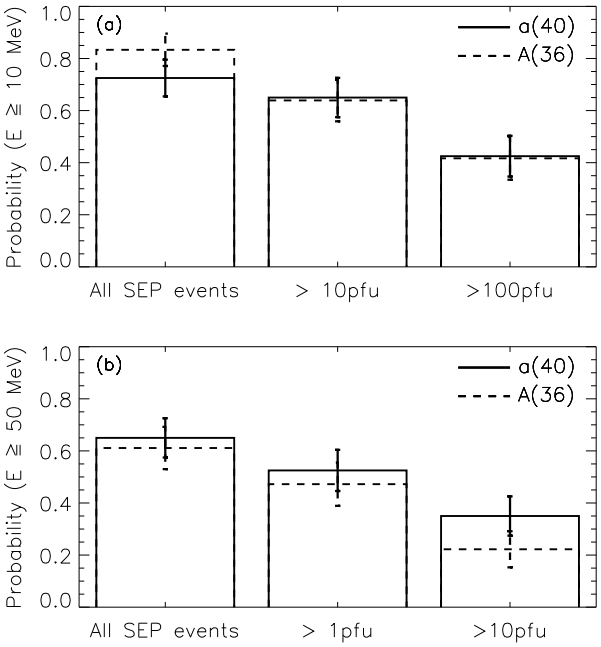

Fig. 4 Occurrence probabilities, P, of SEP events in terms of CH area for proton energies ≥10 MeV (a) and ≥50 MeV(b).

The third and fourth columns of Table 2 show the comparison of CME speed in different groups binarized by CH proximity (group 'd' and 'D'). It is found that the speeds of SEPYCMEs in groups 'd' and 'D' are almost the same. Meanwhile, the speeds of SEPNCMEs in these two groups are also similar. Such results imply that no significant fast CMEs were required for producing SEP events when CMEs are close to CHs. This result is consistent with Kahler (2004)'s result that no significant fast CMEs were required for producing the SEP events in the fast solar wind region.

3.2 Dependence of CH Area

Figure 4 shows the occurrence probabilities, P, of SEP events in terms of the closest-CH area for proton energies ≥10 MeV and ≥50 MeV. For the SEP events with proton energies ≥10 MeV shown

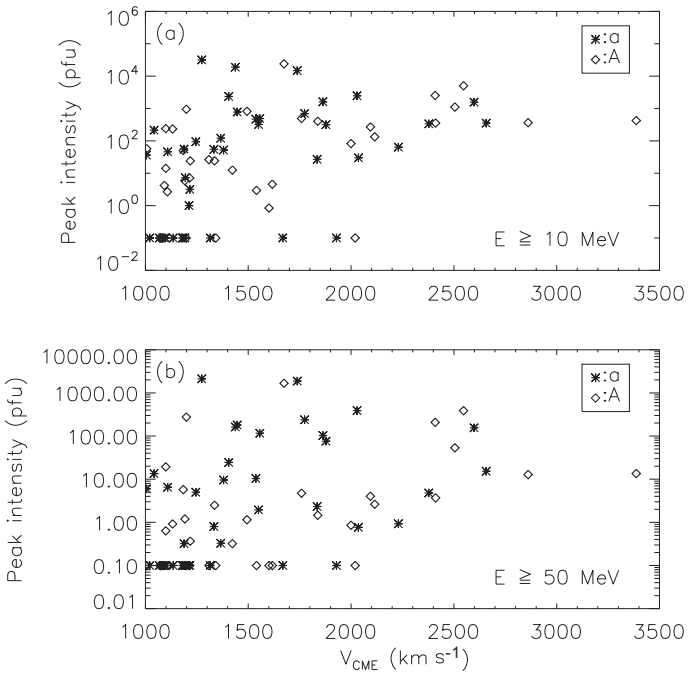

Fig. 5 Peak intensity of proton with energy ≥10 MeV vs. associated CME speed for proton energy ≥10 MeV (a) and ≥50 MeV (b). The asterisks show the CMEs in group 'a' while diamonds show the CME in group 'A'.

in Figure 4(a), the occurrence probabilities of SEP events in group 'A' are smaller than those in group 'a' at large flux levels (≥10 pfu and ≥100 pfu). However, such differences are very small. For the SEP events with proton energy ≥50 MeV (Fig. 4(b)), the occurrence probabilities of SEP events in group 'A' are all smaller than those in group 'a'. The difference between groups 'a' and 'A' for the SEP events with proton energy ≥50 MeV are bigger than those for the SEP events with proton energy ≥10 MeV and became larger with the increase of the flux level. Even so, such differences are still small and less than 1σ. Thus, the areas of the corresponding CHs did not show any evident influence on the CME in generating SEPs.

The peak intensity, which varied with the associated CME speed for groups 'a' and 'A', are shown in Figure 5 while the mean values of the speed of SEPYCMEs and SEPNCMEs are also listed in Table 2 (5th and 6th columns). Similar to the analysis of CH proximity, no obvious difference of CME speed distribution between groups 'a' and 'A' could be found. The mean values of the speed of SEPYCMEs and SEPNCMEs in these two groups are also similar. This result confirms that the area of corresponding CHs shows no evident influence on CME in producing SEP events.

3.3 Dependence of Relative Position

The possible impact of the CHs' location relative to the corresponding CMEs is studied. Figure 6 shows the SEP occurrence probability of CMEs at different flux levels and different energy levels. It is found that the SEP occurrence probability of CMEs at all flux levels and energy levels in group 'Y' are smaller than those in group 'N', especially for the SEP events with flux level ≥10 pfu with proton energy ≥10 MeV, whose SEP occurrence in group 'Y' is much smaller than that in group 'N'. The

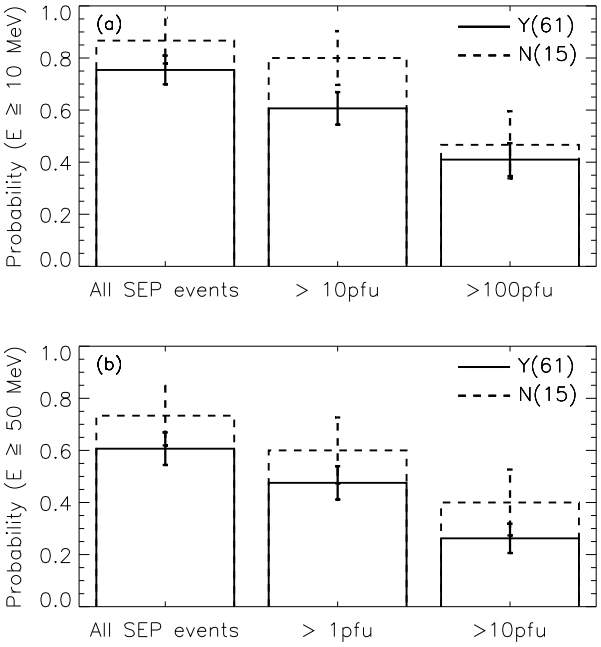

Fig. 6 Occurrence probabilities, P, of SEP events in terms of relative position between CHs and CMEs for proton energies $\geq$10 MeV and $\geq$50 MeV, respectively,

difference between these two groups is larger than 1σ at this level. However, such difference between these two groups is small and less than the value of 1σ for all the other levels. The comparison of the speed of SEPYCMEs for groups 'Y' and 'N' is shown in Figure 7. Similar to the analysis of CH proximity and CH area, no obvious difference of the speed of SEPYCMEs between groups 'Y' and 'N' could be found. The average speed of SEPYCMEs is similar to the average speed of SEPNCMEs as listed in the last two columns of Table 2. These results imply that the relative location of CHs to the corresponding CMEs has no evident effect on SEP events, which is the same conclusion we found in Paper I.

4 SUMMARY AND CONCLUSIONS

In order to study the influence of CHs on CMEs in producing SEP events, a total of 76 west-side fast halo CMEs during 1997 – 2008 are investigated, as well as their associated CHs. Different from the CHs obtained by the brightness method based on EIT 284 Å data in paper I, the CHs that we investigated in this paper are obtained with the aid of the extrapolation of the coronal magnetic field by the CSSS model, in which the MDI daily-updated synoptic magnetic field charts are adopted as the bottom boundary condition. By using this method, all the CHs, defined as the regions consisting of only open magnetic field lines, over the entire solar surface are inferred.

After analyzing three parameters, CH proximity, area of corresponding CHs and relative position between CHs and CMEs, it is found that all of the statistical results do NOT have significance exceeding the 1σ level. These parameters do NOT show any evident influence on SEP occurrence probability, and the speed of SEPYCMEs also do NOT show any difference between different groups

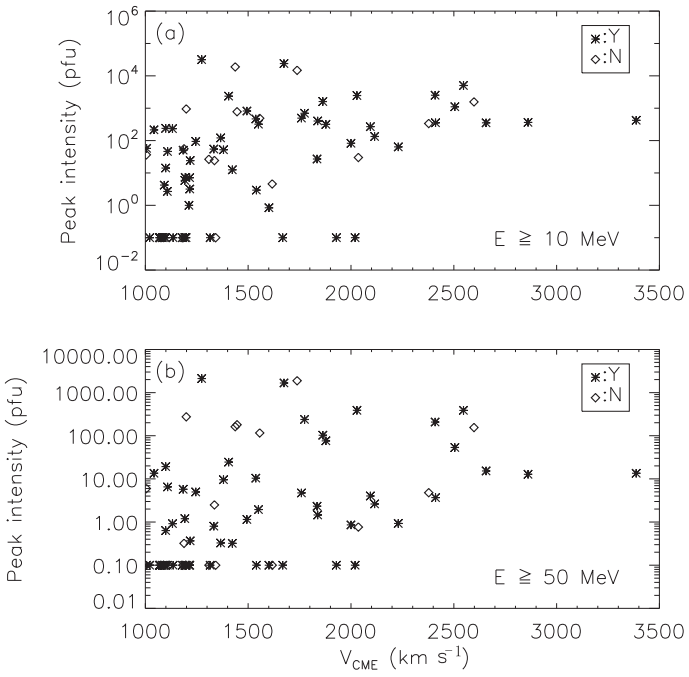

Fig. 7 Peak intensity of proton with energy ≥10 MeV vs. associated CME speed for proton energy ≥10 MeV (a) and ≥50 MeV (b). The asterisks show the CMEs in group 'Y' while diamonds show the CME in group 'N'.

binarized by these parameters. These results confirmed the conclusion we got in Paper I and Kahler (2004) that there was no evident influence of CHs on CMEs in producing SEP events.

An expanding CME may drive a quasi-parallel shock at its flank as discussed by Kahler (2004). The condition of a CME in a driven shock in this situation is only $V_{\rm CME}$ larger than the local Alfv́en speed $V_{\rm a}$ or sound speed $C_{\rm s}$. Thus, the fast flow speed near CHs may show no influence on producing a strong shock. In addition, not only the plasma density but also the magnetic field strength in the fast solar wind region is smaller than those in the slow solar wind region (Ebert et al. 2009), so the Alfv́en speed in the fast solar wind region may not be obviously faster than it is in the slow solar wind region. Based on this analysis, it could be expected that the shock can also be produced in the fast solar wind region near a CH and no evident speed of the CME is needed. In addition, the shock interacting with the background solar wind may generate turbulence. Such turbulence could be treated as the main mechanism that causes particles to go back to the shock acceleration process to produce SEP events (Reames 1999). The closed magnetic topology could only provide an additional method to make the particles go back to engaging in shock acceleration (Shen et al. 2008). So, the influence of open magnetic field topology may be weak in shock producing SEP events.

Acknowledgements We acknowledge the use of data from the SOHO, Yohkoh and GOES spacecraft, as well as the CH maps from the Kitt Peak Observatory. SOHO is a project of international cooperation between ESA and NASA. This work is supported by grants from the National Natural Science Foundation of China (Grant Nos. 40904046, 40874075 and 40525014), the 973 National Basic Research Program (2006CB806304), the Ministry of Education of China (200530), the Program for New Century Excellent Talents in University (NCET-08-0524) and the Chinese Academy of Sciences (KZCX2-YW-QN511, KJCX2-YW-N28 and the startup fund).

References

Altschuler, M. D., & Newkirk, G. J. 1969, Sol. Phys., 9, 131
DeForest, C. E., Lamy, P. L., & Llebaria, A. 2001, ApJ, 560, 490
Ebert, R. W., McComas, D. J., Elliott, H. A., et al. 2009, J. Geophys. Res. (Space Physics), 114, 1109
Fisher, R., & Guhathakurta, M. 1995, ApJ, 447, L139
Gopalswamy, N., Yashiro, S., Akiyama, S., et al. 2008, Ann. Geophys., 26, 3033
Harvey, K. L., & Recely, F. 2002, Sol. Phys., 211, 31
Kahler, S. W. 2004, ApJ, 603, 330
Kunches, J. M., & Zwickl, R. D. 1999, Radiation Measurements, 30, 281
Munro, R. H., & Jackson, B. V. 1977, ApJ, 213, 874
Reames, D. V. 1999, Space Sci. Rev. 90, 413
Schatten, K. H. 1971, Cosmic Eletrodyn., 2, 232
Schatten, K. H., Wilcox, J. M., & Ness, N. F. 1969, Sol. Phys., 6, 442
Scherrer, P. H., Bogart, R. S., Bush, R. I., et al. 1995, Sol. Phys., 162, 129
Shen, C., Wang, Y., Ye, P., Zhao, X. P., Gui, B., & Wang, S. 2007, ApJ, 670, 849
Shen, C. L., Wang, Y. M., Ye, P. Z., & Wang, S. 2006, ApJ, 639, 510
Shen, C. L., Wang, Y. M., Ye, P. Z., & Wang, S. 20068, Sol. Phys, 252, 409
Zhao, X. P., & Hoeksema, J. T. 1992, Eur. Space Agency Spec. Publ., ESA SP-348, 117
Zhao, X. P., & Hoeksema, J. T. 1994, Sol. Phys., 151, 91
Zhao, X. P., & Hoeksema, J. T. 1995, J. Geophys. Res., 100, 19
Zhao, X. P., Hoeksema, J. T., & Rich, N. B. 2002, Adv. Space Res., 29, 411
Zirker, J. B. 1977, Reviews of Geophysics and Space Physics, 15, 257